International Journal of Nanomedicine Dovepress

Open Access Full Text Article ORIGINAL RESEARCH

Chlorogenic Acid-Cucurbit[n]uril Nanocomplex Delivery System: Synthesis and Evaluations for Potential Applications in Osteoporosis Medication

Yunqing Jiang[1,*], Haowen Qi[2,*], Mingjuan Wang[1], Kai Chen[3], Chen Chen[1], Haifeng Xie[2]

[1]Department of Endodontics, The Affiliated Stomatological Hospital of Nanjing Medical University, State Key Laboratory Cultivation Base of Research, Prevention and Treatment for Oral Diseases, Jiangsu Province Engineering Research Center of Stomatological Translational Medicine, Nanjing, 210029, People's Republic of China; [2]Department of Prosthodontics, The Affiliated Stomatological Hospital of Nanjing Medical University, State Key Laboratory Cultivation Base of Research, Prevention and Treatment for Oral Diseases, Jiangsu Province Engineering Research Center of Stomatological Translational Medicine, Nanjing, 210029, People's Republic of China; [3]Collaborative Innovation Center of Atmospheric Environment and Equipment Technology, Jiangsu Key Laboratory of Atmospheric Environment Monitoring and Pollution Control, School of Environmental Science and Engineering, Nanjing University of Information Science and Technology, Nanjing, 210044, People's Republic of China

*These authors contributed equally to this work

Correspondence: Chen Chen, Department of Endodontics, The Affiliated Stomatological Hospital of Nanjing Medical University, State Key Laboratory Cultivation Base of Research, Prevention and Treatment for Oral Diseases, Jiangsu Province Engineering Research Center of Stomatological Translational Medicine, Nanjing, 210029, People's Republic of China, Tel +8625 69 593 031, Fax +8625 86 516 414, Email ccchicy@njmu.edu.cn; Haifeng Xie Department of Prosthodontics, The Affiliated Stomatological Hospital of Nanjing Medical University, State Key Laboratory Cultivation Base of Research, Prevention and Treatment for Oral Diseases (Nanjing Medical University), Jiangsu Province Engineering Research Center of Stomatological Translational Medicine, Nanjing, 210029, People's Republic of China, Tel +8625 69 593 081, Fax +8625 86 516 414, Email hfxie@njmu.edu.cn; xhf-1980@126.com

Purpose: Based on nanomedicine strategies, this study employed cucurbit[7]uril (Q[7]) as the macromolecular carrier to synthesize nanocomplex drug delivery system for chlorogenic acid (CGA). The nanocomplex drug delivery system is intended to overcome the unsatisfactory biocompatibility and bioavailability of CGA and realizing its potential role in long-term osteoporosis (OP) medication.

Methods: The nanocomplex was synthesized by the reflux stirring method. The chemical structure of the nanocomplex was characterized by Fourier transform infrared spectroscopy (FTIR), thermogravimetric analysis (TGA), X-ray diffraction analysis (XRD), UV-visible spectrophotometry (UV-vis), zeta potential analysis and transmission electronic microscope (TEM). The Cell Counting Kit-8 (CCK-8) assay, Live/Dead staining assay, and cytoskeleton staining were conducted to testify the biocompatibility of the nanocomplex. The release assay, Ferric Reducing Ability of Plasma (Frap) assay and Reactive oxygen species (ROS) staining were implemented to evaluate the release profile of CGA as well as its remaining antioxidative levels.

Results: CGA and Q[7] formed hydrogen bonding through an exclusion interaction, with the binding ratio more than 1:1. The nanocomplex had a crystalline and spherical-like structure and improved thermal stability. The nanocomplex demonstrated better biocompatibility than free CGA. The release profile of CGA from the nanocomplex was much steadier, and 70% of CGA was released in 5 days. The CGA released from the nanocomplex maintained its antioxidative properties at high levels and effectively eliminated the accumulated ROS in MC3T3-E1 cells under oxidative stress.

Conclusion: Q[7] has been demonstrated to be an ideal nanocarrier for CGA and the nanocomplex delivery system holds the potential for the long-term medication strategy of OP.

Keywords: Osteoporosis medication, Chlorogenic acid, Cucurbit[n]uril, Nano drug delivery system, Chemical analysis

Introduction

Osteoporosis (OP) is a chronic and progressive skeleton disorder that severely impacts people's quality of life. OP is characterized by increased bone adsorption, decreased bone mineral density, deterioration of bone tissue microstructure, and increased risks of bone fracture.[1] OP is the result of bone remodeling imbalance in which the new bone matrix fails to replace the removed old bone. At the tissue level, bone formation is dependent on the recruitment of sufficient

Received: 5 September 2024
Accepted: 31 October 2024
Published: 9 November 2024

Graphical Abstract

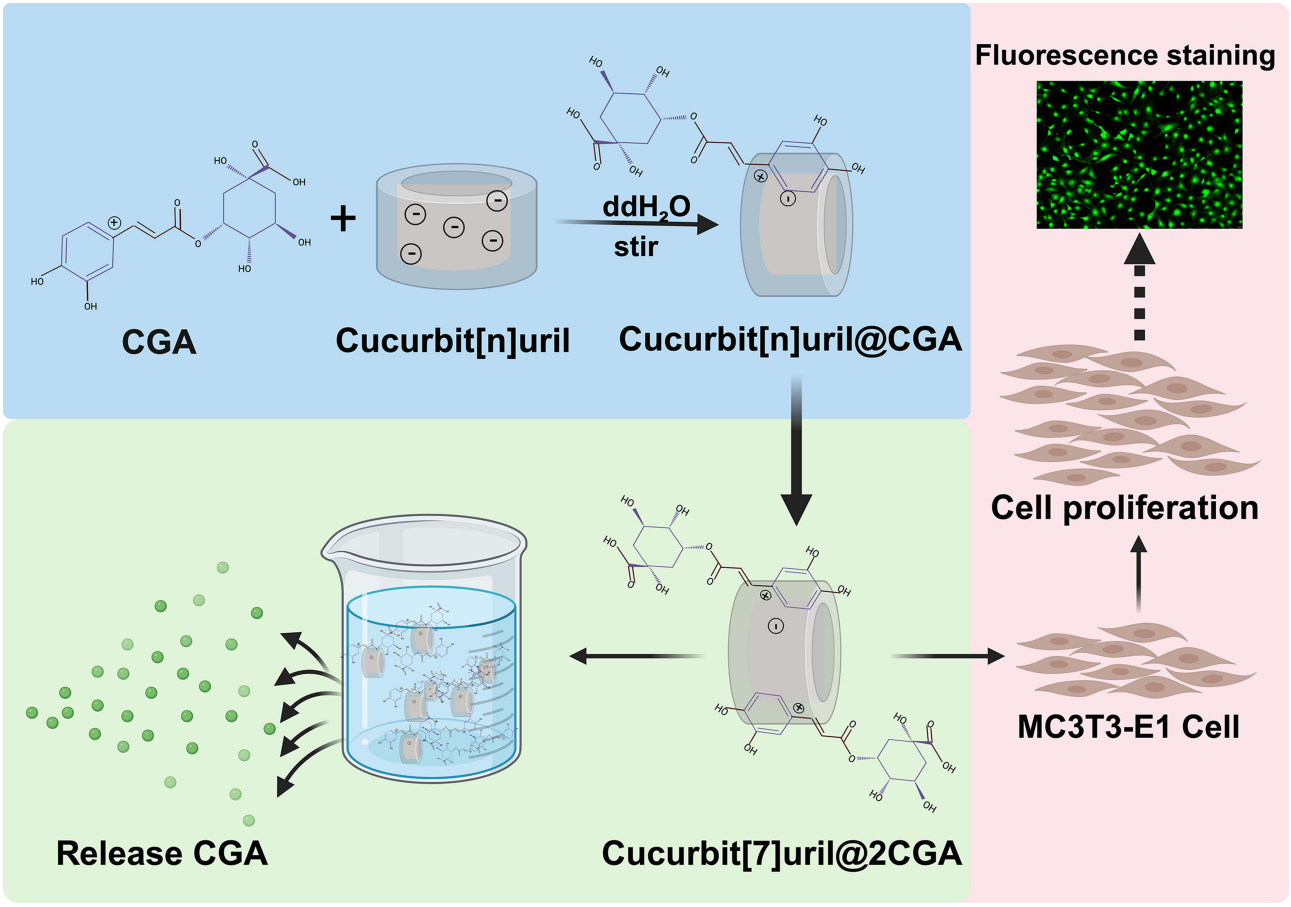

bioactive osteoblasts. The reduced osteoblastic bone formation was caused by a decrease in the quantity and activity of individual osteoblasts, resulting in fewer newly produced bone trabeculae. Therefore, drugs that directly target osteoblast processes are particularly effective in treating OP and strengthening bones.[2,3] Attention has been drawn to the curative effects of natural compounds on OP.[4] Chlorogenic acid (CGA; Scheme 1, left), a polyphenolic compound formed from the esterification of caffeic acid and quinic acid,[5] possesses multiple biochemical functions such as anti-inflammation,[6] antioxidation,[7] immunological modulation,[8] antivirus,[9] etc. It is acknowledged as a potential therapeutic agent for various degenerative diseases. CGA also exhibits modulations for bone homeostasis, as previous research has demonstrated that CGA can promote adhesion and proliferation of osteoblasts.[10] All the evidence reveals that CGA is a promising bone-inducing drug, and may be more suitable for long-term medication than traditional pharmacological methods due to its natural characteristics.[11,12] Nevertheless, developments in CGA-based therapeutic drugs are faced with challenges in biocompatibility and bioavailability.[13,14] Reactive oxygen species (ROS) accumulating in the microenvironment is considered as a great threat. Overproduction of ROS cause lipid and protein oxidation as well as damage the integrity of mitochondrial and nuclear DNA, thereby becoming a key player in OP. High levels of ROS generate oxidative stress in osteoblasts, resulting in decreased adhesion, inferior differentiation, and increased apoptosis. This highlights the necessity of effective antioxidant strategies in recovering mitochondrial dysfunction, enhancing the OP microenvironment, and encouraging osteoblastic repair.[15,16] The biochemical effects of CGA are mainly determined by its phenolic hydroxyl groups, and the reducibility of hydroxyl groups endows CGA with antioxidant capacity, which can effectively eliminate excessive ROS in the microenvironment. However, the application of CGA is also limited by the instability of

its hydroxyl groups, and premature oxidation of hydroxyl groups (caused by pH value, temperature, light, and oxidants) can weaken the antioxidant capacity of CGA.[17] In addition, the high-dose toxicity of CGA cannot be ignored. Research has found that CGA at high doses of 200 μM and 400 μM leads to varying degrees of cytotoxicity in MC3T3-E1 cells at 48 hours.[18,19] A corresponding delivery system should therefore be developed.

Nanonization is considered to be a promising approach to improving the biocompatibility and bioavailability of drugs and achieving controlled release simultaneously.[20,21] Nanodrugs have enhanced drug loading capacity, higher stability, and significantly prolonged blood half-lives.[22] The modifiable forms and diverse surface features allow them to target multiple tissues.[23,24] Moreover, these nanodrugs can be directly applied or incorporated into macromaterials like scaffolds, implants, hydrogels, etc. to solve more complicated osteoporotic bone defects.[25] Nanocomposites consist of two or more materials, in which macromolecular polymers act as main molecules or carriers to accommodate the activity of small molecules.[26–28] This is a widely used nanonization strategy. Macrocyclic main molecules have been widely used in chemistry and medicine due to their unique cavity structure, molecular recognition ability, and drug delivery ability since their first appearance in the 1960s. The first-generation macrocyclic molecule, crown ether, is highly toxic, and its application in medicine is limited.[29] Cyclodextrin is the second-generation macrocyclic main molecule with good water solubility, but it still has low toxicity, and the opening size at both ends of the cavity is inconsistent, which has certain spatial structure requirements for guest molecules.[30]

Therefore, cucurbit[n]urils (Q[n]) (Scheme 1, right), was introduced as the main body for CGA delivery. Q[n] is a cage compound consisting of different glycosidic urea units linked by a methylene unit.[31] The openings at both ends are hydrophobic, small, and surrounded by carbonyl groups of the same size.[32] The host-guest effect of Q[n] can be easily realized,[33] and Q[n] is reported to have good biocompatibility.[34,35] Cucurbit[6]uril (Q[6]) has a cavity volume of 164 $Å^3$ and is known to form stable complexes with fatty amines.[36] Q[7], with a cavity volume of 279 $Å^3$, has a cavity size suitable for encapsulating rather large guest molecules and a greater water solubility relative to other members of the Q[n] family, making it compatible with peptides, proteins, and other biomolecules.[37] Both Q[6] and Q[7] are thus speculated to have the potential to carry CGA.

In the study, the nanocomplexes were synthesized by combining Q[6] or Q[7] with CGA, wherein the concentration of CGA was determined based on the concentration-dependent analysis of CGA cytotoxicity. Fourier transform infrared spectroscopy (FTIR), thermogravimetric analysis (TGA), X-ray diffraction analysis (XRD), UV-visible spectrophotometry (UV-vis), zeta potential analysis and transmission electronic microscope (TEM) were employed to characterize the nanocomplexes and the form of chemical bond between CGA and Q[n]. The bioactivity of the CGA released from the nanocomplexes was determined using Ferric Reducing Ability of Plasma (FRAP) method. The biocompatibility of the nanocomplexes on MC3T3-E1 cells were evaluated using the Cell Counting Kit-8 (CCK-8) assay, Live/Dead staining and cytoskeleton staining. The intracellular ROS levels were evaluated to further confirm the improved bioavailability of the nanocomplex. The hypothesis was that stable chemical bonds can be formed between Q[n] and CGA, thus endow the advantages of improving the release kinetics, bioavailability and biosafety of CGA.

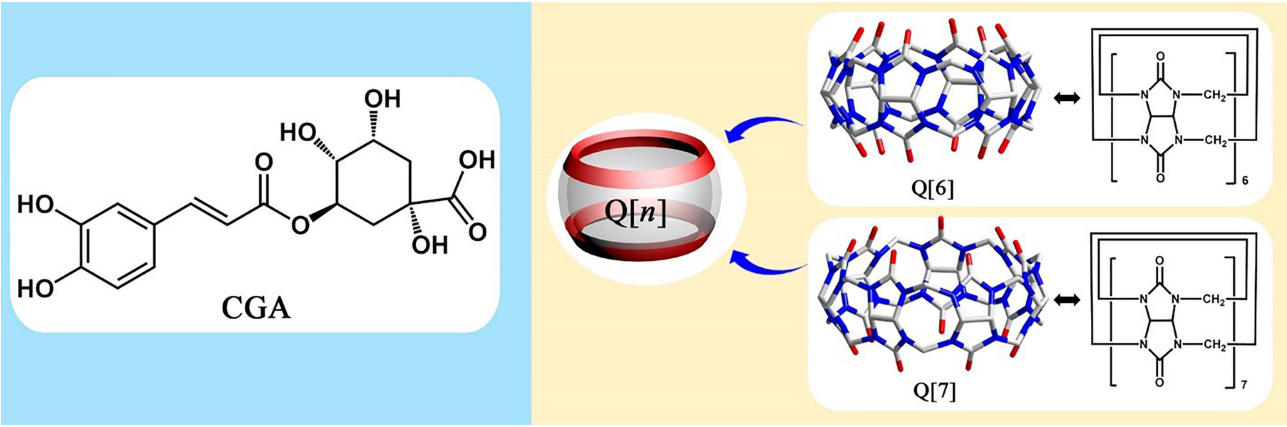

Scheme 1 The structures of chlorogenic acid (CGA; left) and cucurbit[6, 7]uril (right).

Materials and Methods

Concentration-Dependent Analysis of CGA Cytotoxicity

Mouse MC3T3-E1 cells (Chinese Academy of Sciences, China) were cultured in α-minimum essential medium (α-MEM; Gibco, USA) supplemented with 10% fetal bovine serum (Cell Sciences, USA) and 1% penicillin/streptomycin solution (Gibco, USA), and placed in an incubator containing 5% CO_2 at 37°C.

Different concentrations of CGA solutions were filtered using 0.2 μm filters to remove bacteria. The MC3T3-E1 cells were inoculated into 96-well plates at a density of 2000 cells/well (treated with CGA concentrations of 50 μM, 100 μM, 150 μM, 200 μM, 250 μM, and 300 μM) and one control group (treated with the medium), and five replicates were set. The stimulation solution was supplemented after 8 hours of cell attachment. After 24 h, 72 h, and 120 h of culture, the CCK-8 kit (Dojindo Molecular Technology, Kumamoto, Japan) was used to detect the cell proliferation rate and evaluate the cytotoxicity. Absorbance values at 450 nm were measured using a micro-plate spectrophotometer (PerkinElmer, Waltham, MA, USA).

Preparation and Characterization of the CGA-Q[N] Complexes

Self-synthesized Q[6] and Q[7] were separately weighed with a molar ratio of 1:1 to CGA (98%; Aladdin, China). Q[n] (20 mg) was first dispersed in 40 mL of deionized water, and CGA was added to the Q[n] dispersion system, followed by reflux stirring for 8 h at 85°C. Unbound CGA was removed via triplicate washes with anhydrous ethanol, and the obtained wet products denoted as Q[6@CGA] and Q[7]@CGA, were freeze-dried using an LSC Basic freeze-dryer (CHRIST, Germany). A sample with a Q[7] to a chlorogenic acid molar ratio of 1:2 was prepared using the same method and denoted as Q[7]@2CGA. The combination model of Q[7] and CGA is shown in Scheme 2.

FTIR (Nicolet 6700, Thermo Scientific, Waltham, USA) was used to verify the changes in the characteristic peaks of the chemical bonds for CGA, Q[6], Q[7], Q[6]@CGA, and Q[7]@CGA. The infrared spectra were recorded between the 4000 cm^{-1} and 500 cm^{-1} spectral ranges, with the attenuated total reflectance set at 4 cm^{-1} resolution and 32 scans.

In the TGA (TGA-4000, PerkinElmer, Waltham, USA) test, approximately 5 mg of each dried powder sample was placed in a platinum crucible and heated from 28°C to 700°C at a rate of 15°C·min^{-1}. Six samples, CGA, Q[6], Q[7], Q[6]@CGA, Q[7]@CGA, and Q[7]@2CGA, were determined; the sample residual mass percentage (weight%) was calculated and the mutation inflection point was analyzed.

Q[7]@CGA and Q[7]@2CGA were submitted to XRD, host-guest titration UV-vis, DLS analysis, Zeta potential analysis, and TEM. Using XRD (D8ADVANCE, Bruker, Karlsruhe, Germany), the Q[7]@CGA and Q[7]@2CGA complexes trace powders were characterized at room temperature (target, Cu-Ka; scanning speed, 2 °/min; sampling time, 1 s; scanning range, 4–54 °/min). UV titration was performed using a UV-vis (LAMBDA1050+, PerkinElmer, USA). The DLS and Zeta potential were detected using a laser particle sizer (Zetasizer NANO ZS90, Malvern, UK) and phosphate-buffered saline (PBS) to configure the powder samples into a 10^{-4} M solution. TEM (Talos f200s 200 kV, FEI, USA) was used to observe the morphology of the samples at an accelerating voltage of 200 kV.

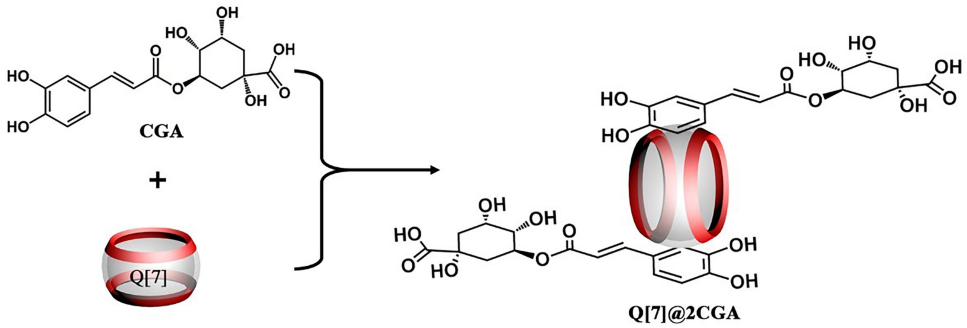

Scheme 2 The potential mechanism of action of Q[7] and CGA.

Slow-Release and Antioxidant Properties of CGA

Phosphate Buffered Saline (PBS; Bioshark, China) was used as a solvent to configure the CGA solutions (concentrations of 10, 20, 40, 60, 80, 100, 120, 160, and 200 μM). A micro-ultraviolet spectrophotometer (NanoDrop One, Thermo, USA) was used to determine the absorbance value of the sample at 329 nm, and the absorbance-concentration standard curve of CGA was obtained.

The Q[7]@CGA, Q[7]@2CGA powders (25 mg each) and physically mixed CGA (11.6 mg)-Q[7] (19.2 mg) powder were dissolved in 5 mL PBS respectively and placed in dialysis bags (Spectrum, In Biotech CE,100–500 Da, USA). The dialysis bag was placed in 200 mL PBS, and 1 mL of liquid was removed from the solution outside the bag every 24 h and 1 mL of PBS was added. The absorbance value of the sample at 329 nm was determined for 20 consecutive days, and the corresponding CGA concentrations were obtained using the standard curve.

The FRAP (Ferric Reducing Ability of Plasma) kit (Beyotime, China) was used to determine the antioxidant activities of the samples in parallel with the sustained release. 100 μL of the above-mentioned extracted liquid was mixed with 200 μL of the FRAP working solution and reacted for 5 min. The absorbance of the mixture was measured using a microplate spectrophotometer (PerkinElmer, USA) at 593 nm. The antioxidant activities were calculated based on a standard curve of absorbances of aqueous $FeSO_4$ at various concentrations (0.15–1.5 mm).

Cell Proliferation and Cytotoxicity Evaluation

The complexes were soaked in 75% ethanol in the cell workbench for 2 h to be sterilized, and the CGA solution were filtered using 0.2 μm filters to remove bacteria as before.

MC3T3-E1 cells were inoculated in 96-well plates at a density of 2000 cells/well, and five replicates were set up in the experimental (200 μM Q[7]@CGA and 200 μM Q[7]@2CGA) and control group (200 μM free CGA). The stimulation solution was replaced after 8 hours of cell attachment. After 24, 72, and 120 h, the CCK-8 kit was used to detect the cell proliferation rate and evaluate the cytotoxicity. The absorbance was measured at 450 nm using a microplate spectrophotometer.

MC3T3-E1 cells were inoculated in 24-well plates at a density of 2×10^4 cells/well. The experimental and control groups were set up as described for the CCK-8 experiment, with three wells in each group. The stimulation solution was replaced after 8 hours of cell attachment. After 72 h of culture, the cell morphology was observed under an inverted fluorescence microscope (LSM 780, CalZeiss AG, Germany) after fluorescent staining with 4, 6-diamino-2-phenylindole (Apexbio, USA) and Ghost Pen Cyclic Peptide (Cytoskeleton, USA). Similarly, the cell viability was observed under an inverted microscope after fluorescent staining with Calcein-AM (Beyotime, China) and propidium iodide (PI; Beyotime, China).

Intracellular ROS Evaluation

MC3T3-E1 cells were inoculated in 96-well plates at a density of 4000 cells/well. 300 μM H_2O_2 was added to the culture medium to induce oxidative stress. After 72 h of coculture, the intracellular ROS levels were evaluated using the DCFH-DA probe kit (Beyotime Institute of Biotechnology, China). The cells were washed three times and incubated with DCFH-DA solution for 20 minutes. ROS fluorescence signals were observed using an inverted fluorescence microscope (ZEISS).

Statistical Analysis

All the experiments were performed at least in triplicate in the study. Statistical analyses were conducted by the GraphPad software (San Diego, CA). One-way analysis of variance (ANOVA) was performed and values of $p < 0.05$ indicated a significant difference. Data were expressed as the mean ± standard deviation.

Results

Concentration-Dependent Analysis of CGA Cytotoxicity

Figure 1 shows the CCK-8 results of MC3T3-E1 cells treated with different concentrations of CGA for 24–120 h. Cell proliferation was enhanced at a concentration of 50 μM for 24 h, with no significant differences between the control

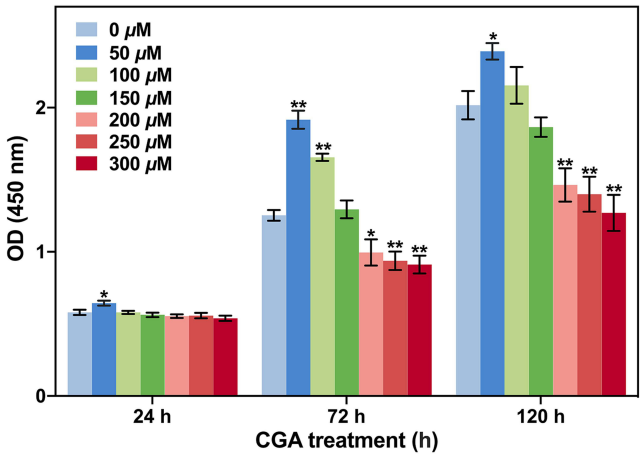

Figure 1 The optical density (OD) values were measured using the CCK-8 Cell Counting Kit after treatment of MC3T3-E1 cells with different concentrations of CGA for 24, 72 and 120 hours. *p < 0.05 and **p < 0.01 indicate significant differences compared to the blank group.

group and groups at higher concentrations. Cell proliferation increased in the 50 μM and 100 μM groups after 72 h but was inhibited dramatically at concentrations over 150 μM. After 120 h of culture, only the 50 μM group demonstrated an improvement in OD value, whereas concentrations beyond 200 μM negatively impacted cell growth. Based on the above results, 200 μM CGA was selected as the toxic concentration for CGA in subsequent experiments.

Characterizations of the CGA-Q[7] Complexes

The results of the infrared analysis are shown in Figure 2A. CGA demonstrated an O-H stretching vibration at 2954 cm^{-1}, Q[7] demonstrated an O-H stretching vibration at 2931 and 3001 cm^{-1}, and the O-H stretching vibration of Q[7]@CGA was observed at 2927 cm^{-1}. The dual vibration peaks of Q[7] fused into a single vibration peak similar to

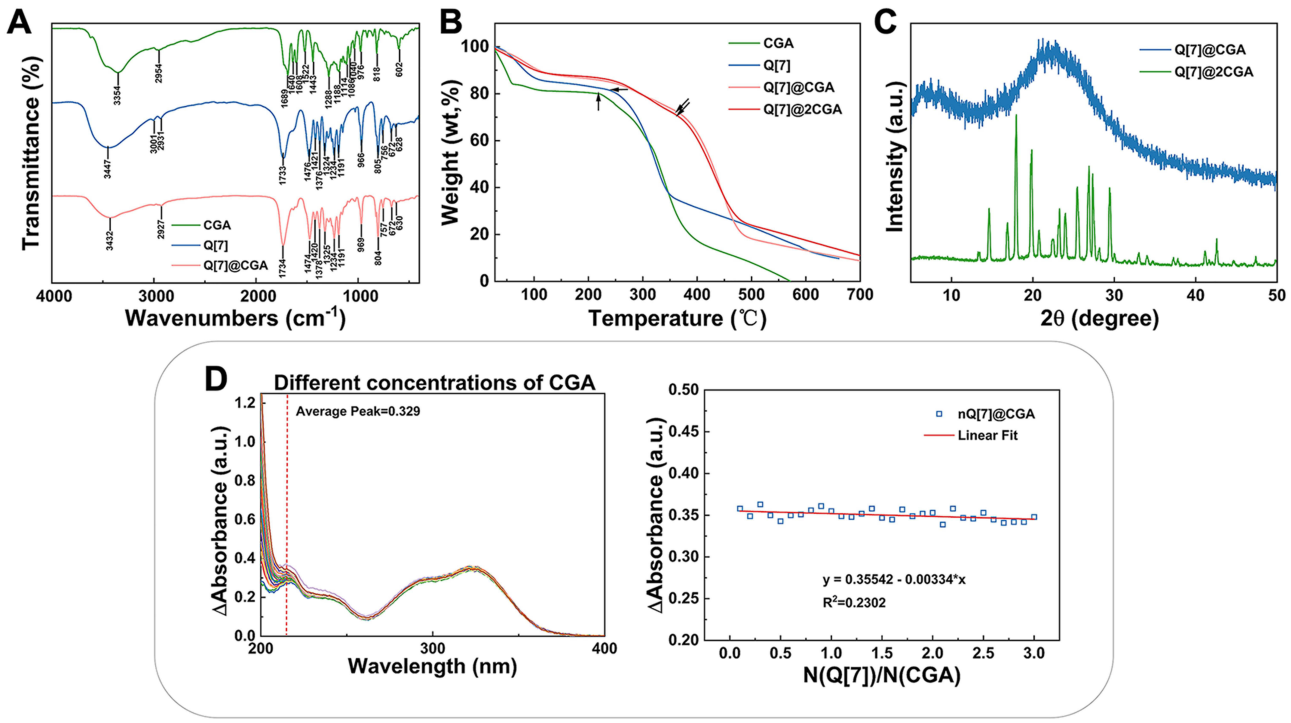

Figure 2 FTIR, TGA, XRD, and UV-vis results of CGA, Q[7], and the complexes. (**A**) FTIR spectra of CGA, Q[7], and Q[7]@CGA. (**B**) TGA curve of CGA, Q[7], and Q[7]@CGA. (**C**) XRD patterns of Q[7]@CGA and Q[7]@2CGA. (**D**) UV standard curve of CGA; the host-guest titration UV analysis of CGA, Q[7], and Q[7]@CGA.

CGA. The hydroxyl vibration peak of Q[7]@CGA was slightly higher than that of Q[7], indicating that Q[7] and CGA may chemically bind by changing the hydroxyl group.

The results of the thermogravimetric analysis (Figure 2B) and heat release (Figure S4) for CGA, Q[7], Q[7]@CGA, and Q[7]@2CGA showed that 16% of the first segment weight loss of CGA occurred at 0–59°C and 68% of the rapid weight loss occurred at 221–401°C, which was due to the collapse of the long carbon backbone in CGA. In the case of Q[7], 14% weight loss in the first segment occurred at 0–105°C, and 44% rapid weight loss occurred at 237–350°C. An 11% weight loss in the first segment of Q[7]@CGA occurred at 0–123°C, and 54% rapid weight loss occurred at 366–481°C. Likewise, a 10% weight loss in the first segment of Q[7]@2CGA occurred at 0–124°C, and 50% rapid weight loss occurred at 368–490°C. The second segment weight loss inflection points of the complexes were significantly higher than those of CGA and Q[7]. The TGA images of Q[7]@CGA and Q[7]@2CGA almost overlapped, indicating that the results of both methods of Q[7]@CGA and Q[7]@2CGA are Q[7]@2CGA.

Figure 2C shows the wide-angle XRD patterns of Q[7]@CGA and Q[7]@2CGA. Q[7]@CGA exhibited a non-crystalline structure, suggesting an amorphous phase, while Q[7]@2CGA exhibited a crystalline structure.

Figure 2D shows the UV standard curve of CGA and the host-guest titration UV analysis of CGA, Q[7] and Q[7]@CGA. When CGA was titrated with Q[7], the characteristic peak of CGA was always observed within the UV spectrum; thus, the interaction between Q[7] and CGA may be considered as an exclusion interaction rather than an inclusion interaction.

As seen in Figure 3A, the particle size of CGA was distributed within the range of 122.4–133.8 nm, and that of Q[7] was mainly distributed within the range of 162.2–175.8 nm. The particle sizes of the Q[7]@CGA and Q[7]@2CGA complexes were distributed within the ranges of 229.5–243.9 nm and 399.5–411.8 nm, respectively. The particle size of Q[7] combined with CGA was slightly larger than that of Q[7] or CGA alone, and the particle size of Q[7]@2CGA was larger than that of Q[7]@CGA.

The Zeta potential is a measure of the strength of the mutual repulsion or attraction between particles, and the bigger the absolute value of the Zeta potential, the better the stability of the particle. The Zeta potential distribution of CGA, Q[7], Q[7]@CGA, and Q[7]@2CGA is shown in Figure 3B. The Zeta potential values for CGA, Q7, Q[7]@CGA, and Q[7]@2CGA were −2.17 mV, +30.9 mV, +26.2 mV, and +19.7 mV, respectively.

The powdered appearances of Q[7], CGA, Q[7]@CGA, and Q[7]@2CGA, which can be distinguished by the naked eye, are shown in Figure 4A. Q[7] was yellowish-white in color, CGA was light yellowish-brown, Q[7]@CGA was yellowish-brown, and Q[7]@2CGA was similar in appearance to Q[7]@CGA. The TEM images of Q[7], Q[7]@CGA, and Q[7]@2CGA at different magnifications (Figure 4B) showed that the Q[7] particles were unevenly dispersed and mostly irregular and spherical, with a diameter of about 50 nm. The Q[7]@CGA particles were also dispersed and irregular in shape, with a diameter ranging from 11 to 80 nm. The Q[7]@2CGA particles were nearly circular with uneven surfaces and a diameter of about 100 nm.

Release Profile and Antioxidants of CGA from the Complexes

Figure 5A shows the cumulative CGA release percentage from free CGA, Q[7]@CGA, and Q[7]@2CGA within 20 days. The release rate of free CGA was fast, reaching 90% at 12 h, and the release amount did not significantly change over the following 20 days. In the Q[7]@CGA and Q[7]@2CGA complexes, the release of CGA can be divided into three phases. In the first 5 days, 69% and 70% of CGA was released, respectively; the release amount then reached 77% and 79%, after a stable and slow release within 6–9 days; the final release reached 80% and 82%, respectively, after 10–20 days. The FRAP method was used to evaluate the remaining antioxidant activities of per mg CGA with Fe^{2+} as a reference. The antioxidant activity of CGA began to decrease on day 10 in group free CGA, but was maintained in the Q[7]@CGA and Q[7]@2CGA groups (Figure 5B).

Cell Proliferation and Cytotoxicity Evaluation

According to the CCK-8 results in Figure 6, the free CGA group showed obvious cytotoxicity from 24 h to 120 h. Both Q[7]@CGA and Q[7]@2CGA promoted the proliferation of osteoblasts, and the effect was more prominent with Q[7]@2CGA. Q[7] did not exhibit any cytotoxicity at 24–120 h.

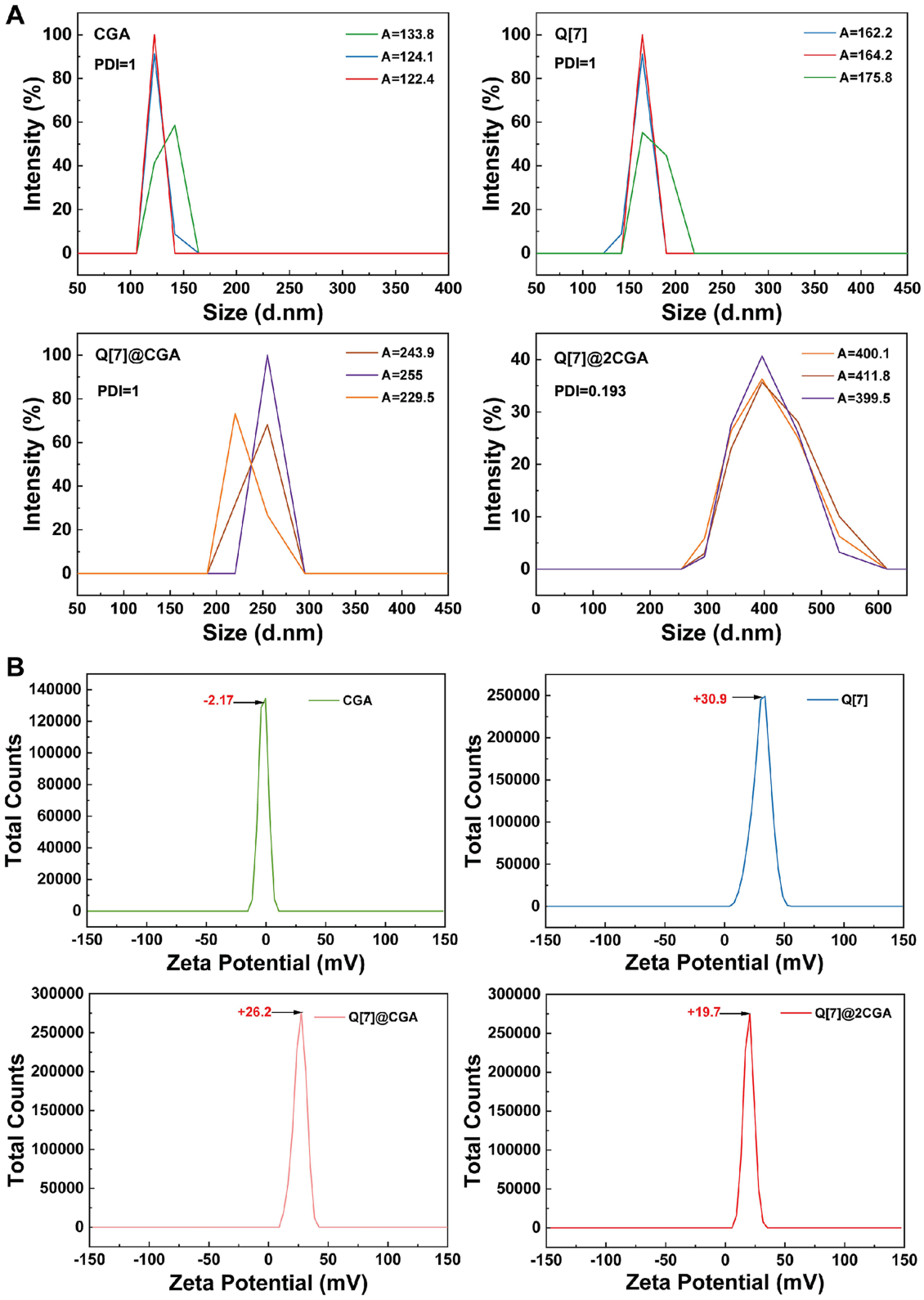

Figure 3 The DLS and Zeta potential distribution. (**A**) DLS results for CGA, Q[7], Q[7]@CGA, and Q[7]@2CGA. (**B**) Zeta potential results of CGA, Q[7], Q[7]@CGA, and Q[7]@2CGA.

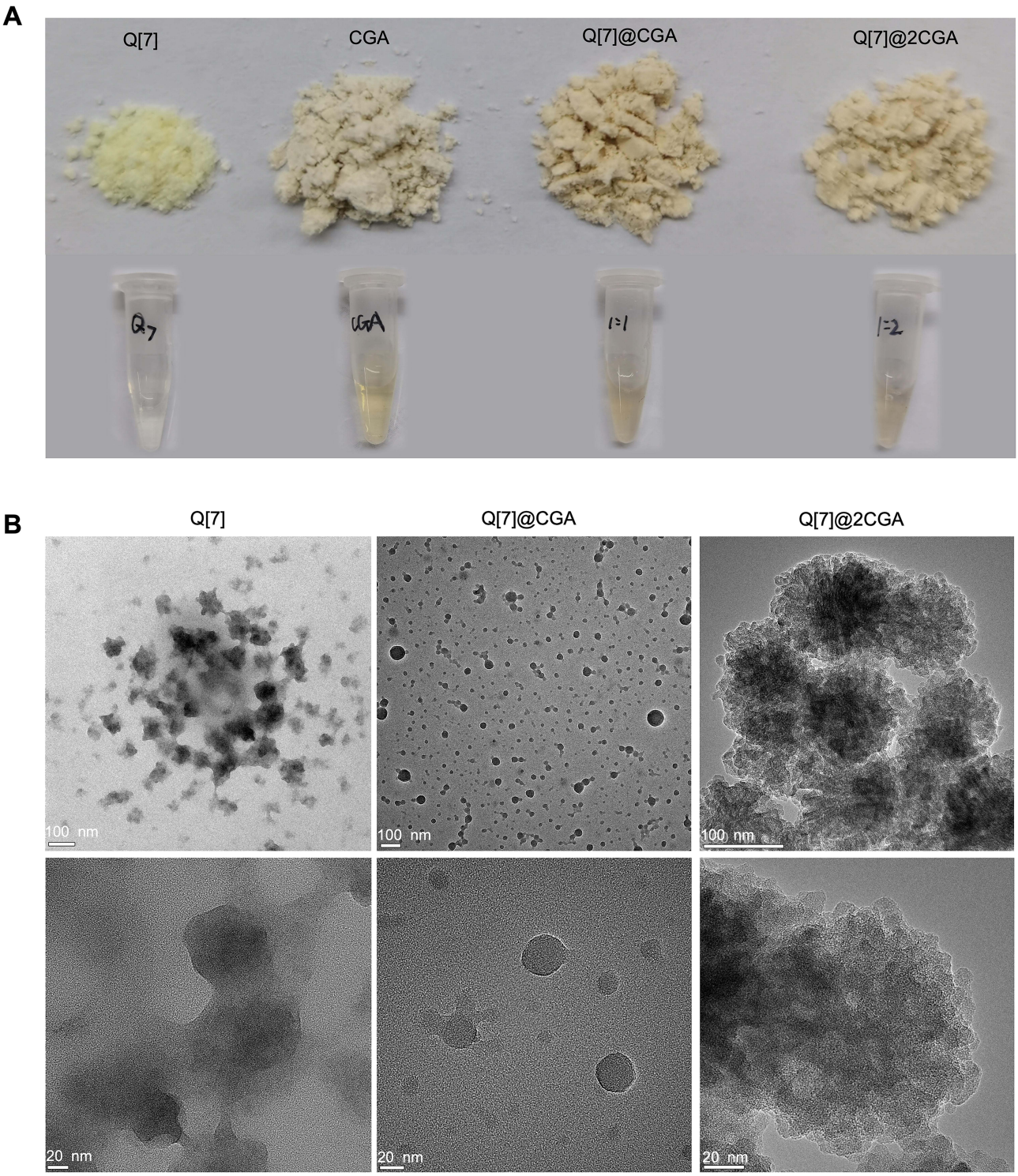

Figure 4 Appearance and TEM results of CGA, Q[7], and the complexes. (**A**) Solid and liquid appearances of CGA, Q[7], Q[7]@CGA, and Q[7]@2CGA; (**B**) TEM images of Q[7], Q[7]@CGA, and Q[7]@2CGA at different magnifications.

Figure 7A exhibited the results of cytoskeleton staining of MC3T3-E1 cells after 3-day coculture. In the CGA group, the cells were fusiform in shape with no obvious cell pseudopods; additionally, they were not well spread out. In the blank, Q[7], Q[7]@CGA, and Q[7]@2CGA groups, the cells were spread out and presented as round-shaped structures with many filaments. The cells in the blank and Q[7]@2CGA groups were the most well-spread.

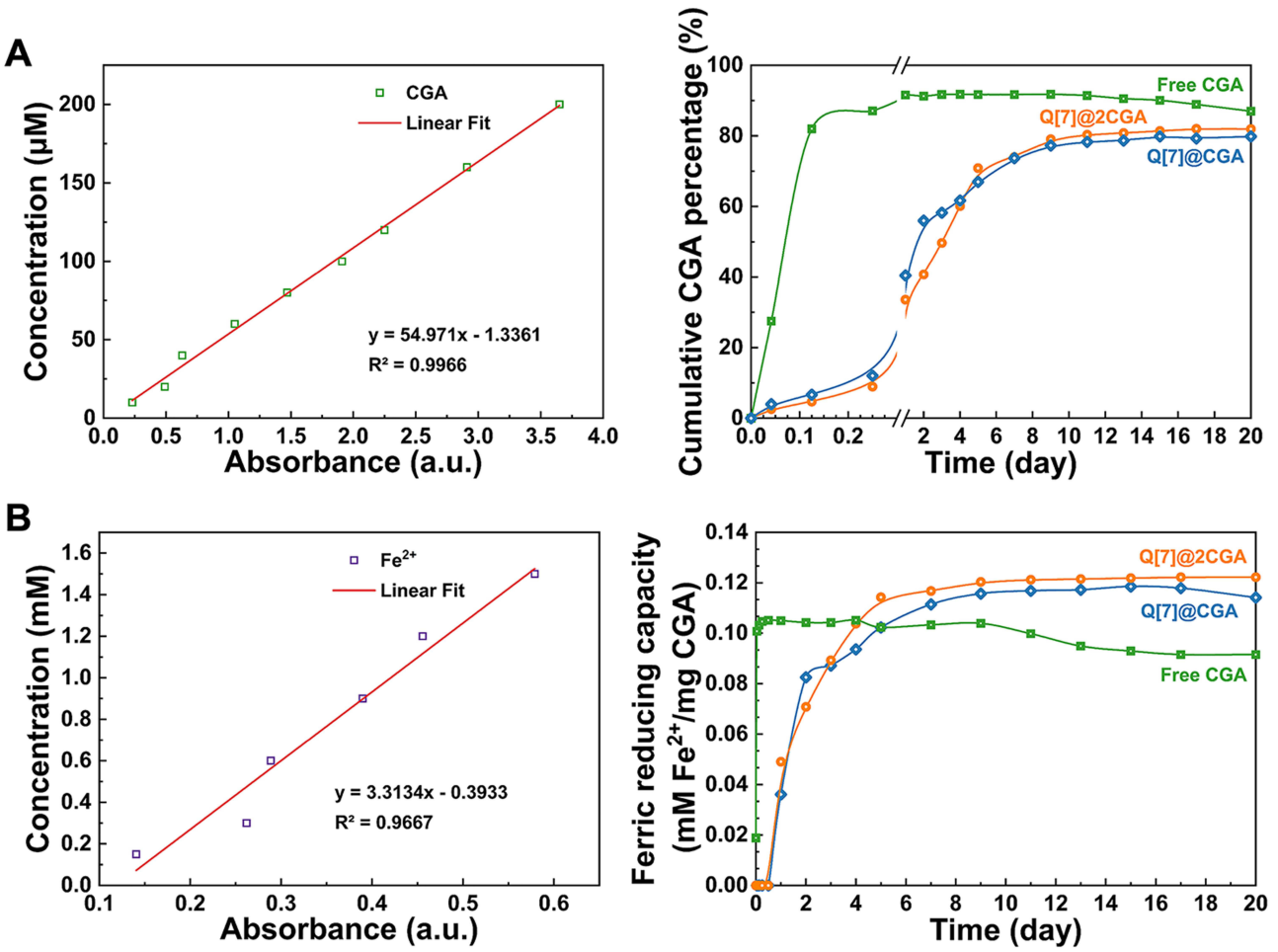

Figure 5 The release profile and antioxidant activity of CGA. (**A**) The absorbance-concentration standard curve and release percentage of CGA from free CGA, Q[7]@CGA, and Q[7]@2CGA; (**B**) Fe^{2+} Reducibility - concentration standard curve and antioxidant activity of the released CGA from free CGA, Q[7]@CGA, and Q[7]@2CGA.

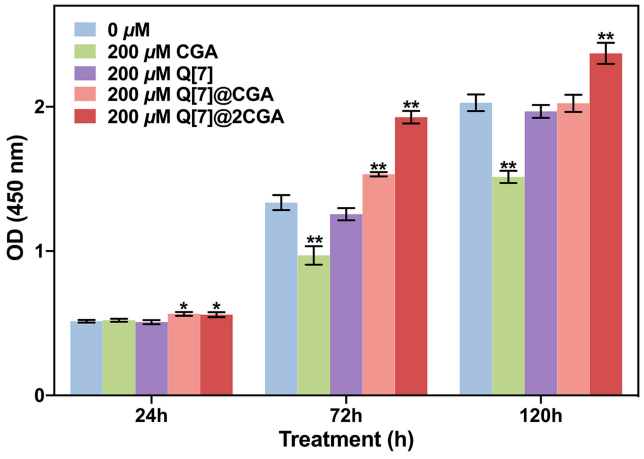

Figure 6 The OD values were measured using the CCK-8 Cell Counting Kit after the treatment of MC3T3-E1 cells with free CGA, Q[7], Q[7]@CGA, and Q[7]@2CGA for 1/3/5 days. *$p < 0.05$ and **$p < 0.01$ represent significant differences compared to the blank group.

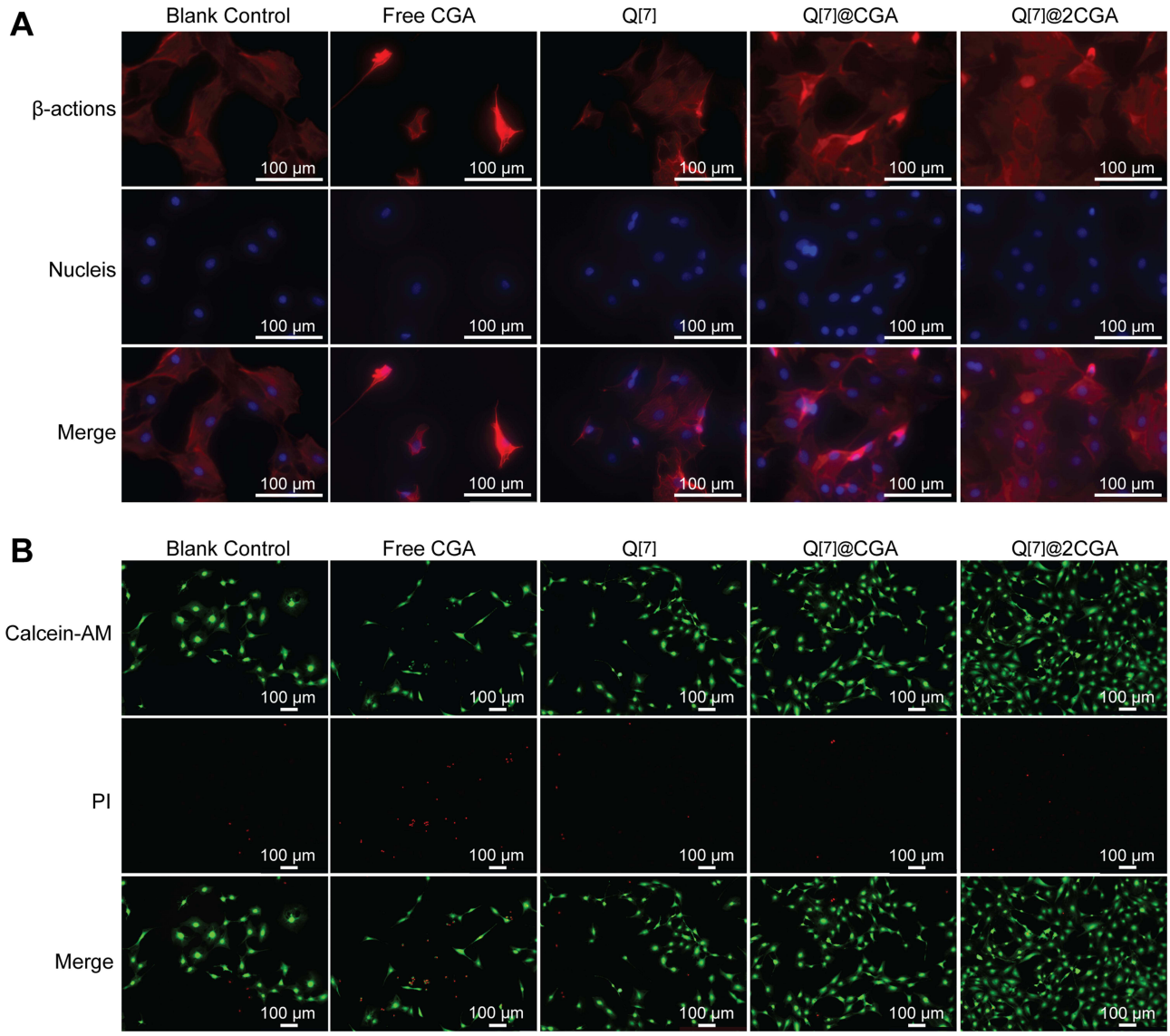

Figure 7 Cell adhesion and comparison of survival and death after treatment with CGA, Q[7], Q[7]@CGA, and Q[7]@2CGA. (**A**) Fluorescence staining of 4, 6-diamino-2-phenylindole with phloxine cyclic peptide and DAPI (Red represents the cytoskeleton, and blue represents the nucleus). (**B**) Fluorescence staining of Calcein-AM and PI (Green is for living cells, red is for dead cells).

The results of Live/Dead cell staining were depicted in Figure 7B. The number of living cells was highest in the Q[7]@2CGA group and lowest in the CGA group. The number of dead cells was highest in the CGA group; the remaining groups presented with low numbers of dead cells.

Intracellular ROS Evaluation

The intracellular ROS levels were shown in Figure 8. In groups blank control and Q[7], strong signals of intracellular ROS triggered by oxidative stress were observed. ROS signals was significantly decreased in groups free CGA, Q[7]@CGA and Q[7]@2CGA. Group Q[7]@2CGA showed the weakest ROS signals among the five groups.

Discussion

The study employed the MC3T3-E1 mouse calvaria-derived pre-osteoblast cell line, which has stable expression patterns of bone-related proteins during osteoblast differentiation and has been extensively studied in investigations over osteoblasts' role in bone formation.[38] The CCK-8 results comparing various concentrations of CGA revealed its

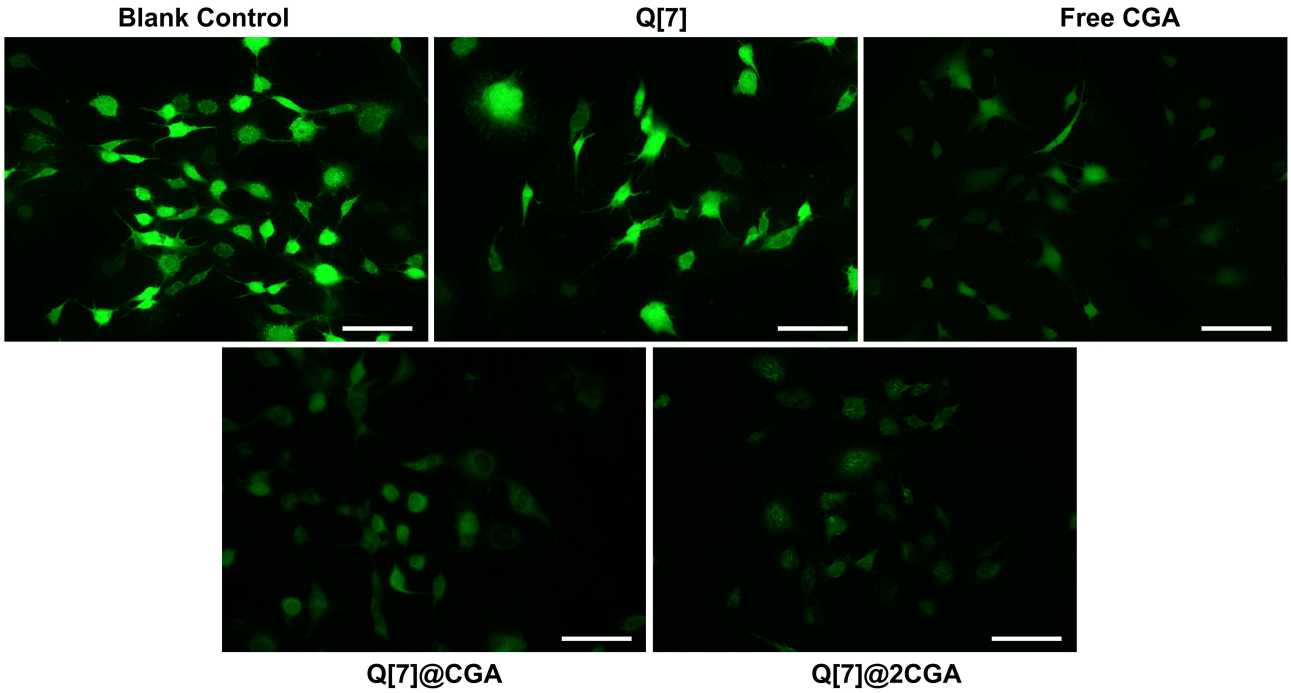

Figure 8 ROS fluorescence signals of cells after treatment with CGA, Q[7], Q[7]@CGA, and Q[7]@2CGA for 3 days under oxidation stress. Scale bar = 100 μm.

concentration-dependent cytotoxicity on MC3T3-E1 cells. High doses will certainly bring stronger bioactivity while inevitably increasing cytotoxicity at the same time, thus impairing the curative effects of CGA in the clinic. 200 μM of CGA (toxic concentration) was selected as the control to evaluate the progress the nanocomplexes made in biocompatibility, since CGA higher than this concentration exhibited significant inhibition on cell proliferation.

The CGA-Cucurbit[n]uril nanocomplexes were synthesized via the reflux stirring method. The diameters of both Q[7]@CGA and Q[7]@2CGA were lower than the simple sum of the diameters of free CGA and free Q[7] in equal proportions, suggesting the formation of nanocomplexes. The nanocomplexes showed no cytotoxicity and even promoted cellular proliferation under inhibitive concentrations. Such a phenomenon can be partially attributed to the sustained-release effect offered by Q[7], which maintained the level of CGA in the microenvironment at a low concentration suitable for cell growth. CGA's cytotoxicity at high concentrations stems from its catechol structure, which generates superoxide anion radical from molecular oxygen by forming an electrophilic o-quinone counterpart, making it act as a pro-oxidant rather than an antioxidant.[39] The outer space interaction between Q[7] and CGA at the location of catechol structure may interfere with the above biochemical process, and the mechanism need to be investigated in future studies. After 5 days of co-culture, it was found that cells in the Q[7]@CGA and Q[7]@2CGA groups exhibited the most developed morphology, with stretched spindle shapes and wide-spread pseudopodia. It is widely accepted that cell morphology plays a vital role in regulating the cell phenotype, and the elongated spindle shape implies better performance in cell adhesion, proliferation, and osteogenic differentiation.[40] Q[6]@CGA complexes were also synthesized and characterized by FTIR and TGA (seen in Supplementary Data: Characterizations of CGA-Q[6] complexes). A weak interaction between CGA and Q[6] was observed (Figures S1 and S2). However, the CCK-8 results (Figure S3) indicated that they did not have the equivalent biocompatibility as Q[7]@CGA. Q[6] itself does not exhibit evident cytotoxicity, but its insolubility in organic solvents and low solubility in water impose limitations on its application. The process of forcefully dissolving Q[6]@CGA in culture medium may have caused damage to Q[6]'s structure and too-fast release of CGA. In light of this, Q[7]@CGA was subjected to further study.

The sustained release of drugs can be realized through drug delivery systems (DDS). In most cases, drugs are confined in carriers with no interactions between them, and the release of drugs is achieved through the degradation of carriers, thereby slowing down the release rate and reducing the accumulative concentrations at target sites.[41] It is

noteworthy that interactions between drugs and carriers will improve carriers' affinity for drugs, promote the stability of DDS, and advance the sustained-release effect. FTIR results provided preliminary evidence for the chemical interactions between the hydroxyl group in CGA and the carbonyl group in Q[7], as Q[7]@CGA demonstrated an enhanced hydroxyl stretch peak at 2927 cm^{-1}. On the other hand, TGA represents a more convincing characterization tactic. The 8% loss of weight in Q[7]@CGA due to water evaporation indicated the occurrence of chemical changes related to OH and/or H during the formation of Q[7]@CGA; thus, hydrogen bonds were formed, which greatly reduced the content of crystal water in the sample. Compared to CGA and Q[7], the inflection point of the complex weight loss shifted significantly to the right, indicating that Q[7]@2CGA was more stable and its main carbon chain could not be thermally decomposed below 360°C. These findings confirmed that stable chemical binding could be formed between Q[7] and CGA through hydrogen bonding, ion-dipole forces, and other chemical forces. Previous studies demonstrated that CGA had a crystalline structure, whereas Q[7] had an amorphous phase.[42,43] UV results revealed that Q[7]@CGA and Q[7]@2CGA formed through exclusion rather than inclusion interaction, which explained the crystalline structure in Q[7]@2CGA. Furthermore, TGA and FTIR data provided evidence that Q[7]@2CGA was more stable than Q[7]@CGA, implying that the CGA linked to the outer wall of Q[7] was more likely to unbind during the washing step, resulting in a non-crystalline Q[7]@CGA.The slow release effects of Q[7]@CGA complexes may be related to the hydrophilicity of CGA; the hydrogen bond of the complex gradually weakens under the hydrophilic action of CGA, and the ion-dipole effect becomes ineffective after the complex potential changes in solution, resulting in the re-release of CGA.[44]

Improving bioavailability is another target we tried to achieve by developing the nanocomplexes. The antioxidant properties of CGA can combat the oxidative stress damage of cells and create an ideal microenvironment for bone regeneration. Nevertheless, the instability of CGA deeply impairs its antioxidant properties and induces the inactivation of CGA earlier than expected. The distribution of drugs in the microenvironment is influenced by their shapes, and the well distribution can partially compensate for the instability of drugs. Evidence has shown that small and spherical molecules can be well transported by blood flow, significantly extending their half-lives.[45] The DLS analyses demonstrated that both Q[7]@CGA and Q[7]@2CGA are nanoscale particles. TEM observations showed that the gap between a single Q[7] particle became smaller in Q[7]@CGA, and the shape of Q[7]@2CGA was more regular and closer to a sphere, which not only implied the binding ratio of CGA and Q[7] larger than 1:1, but also explained the progress in CGA's bioavailability. Q[7] exhibited formless agglomerates, which are typical of amorphous materials, while pure CGA displayed irregular crystal particles with large dimensions.[43] This morphology change from irregular shape to approaching sphere can be explained by the packing meter, which is affected by the hydrophobic component of the molecule. As the CGA content of the nanocomplex grew, so did the hydrophobic component, resulting in a lower packing meter. As a result, greater spherical shape can be observed.[46] The cyclodextrin family is the most commonly used host to synthesize the inclusion of CGA. β-cyclodextrin (β-CD) as the host molecular only reached 79.86% of the inclusion rate for CGA, which is much smaller than that of Q[7]. Besides, the melting point of the complex was lower than that of β-CD and chlorogenic acid, suggesting that the complex was more likely to be thermally decomposed than free CGA, which is not beneficial for improving CGA's bioavailability.[47] The complexation behavior of a more hydrophilic derivative, hydroxypropyl-β-cyclodextrin (HP-β-CD), and CGA was also investigated, but the binding ratio was still limited to 1:1.[48] Both catechol hydroxyl groups of CGA are trapped inside the β-CD cavity, with only the carboxyl moiety projecting outward.[43] The β-CD cavity prevents hydroxyl groups from directly reacting with free radicals and may decrease the efficiency of CGA in the antioxidation process. In cases of Q[7], a different spatial relation was present: the outer surface connection between CGA and Q[7] allowed CGA to be more easily released from the host and exert biochemical activities through its hydroxyl groups. More CGA was released from Q[7]@2CGA at the same total mass as Q[7]@CGA, indicating that Q[7]@2CGA bound more CGA, thus further verifying the structure of the Q[7]@2CGA complex. The absolute Zeta potential values of Q[7]@CGA and Q[7]@2CGA were larger than that of CGA but smaller than that of Q[7], indicating that the stability of the complex in solution was slightly lower than that of free Q[7] but significantly higher than that of free CGA. As a result, CGA in the nanocomplexes may not be easily degraded under the influence of the local microenvironment. Thus, Q[7]@CGA and Q[7]@2CGA were observed to preserve strong antioxidant properties in the FRAP assay and effectively reduce the ROS level in MC3T3-E1 cells.

Most applications of the cucurbit[n]urils family depend on its versatility to form dynamic complexes with various chemicals; however, it is important to understand the binding strengths of the subject molecule and the target guest and the kinetics of the complexation and decomplexation, and make use of those understandings for applications in specific areas.[49,50] The wrapping or loading of cucurbit urea can aid in the specific recognition of molecules, wrapping of toxic functional groups to reduce toxicity, and making of active substances that continue to play a role as a slow-release subject.[51,52] In the current study, cucurbit[*n*]urils were employed to improve the biocompatibility and bioavailability of CGA for its applications in OP treatment. Due to the limitations of the current synthesis method, CGA demonstrated improved biocompatibility, bioavailability, and sustained release via an outer space interaction with Q[7], and future research should focus on allowing CGA to enter the Q[7] cavity to achieve the greatest improvements in the aforementioned aspects. Such nanocomplexes are also promising in bone tissue engineering, particularly when introduced into scaffold material to enhance massive bone defect healing.[53]

It is noteworthy that the strategy of loading active ingredients on cucurbit[n]urils is not only suitable for CGA, but universal for all molecules that can interact with the outer surfaces of cucurbit[n]urils.

Conclusion

Based on the present results, the hypothesis that chemical bonds can be formed between Q[n] and CGA, thus endow the advantages of improving the release kinetics, bioavailability and biosafety of CGA, can be accept, and the following conclusions can be drawn:

i. The novel CGA-Q[7] nanocomplex, based on macrocyclic main molecules, was successfully synthesized through the formation of hydrogen bonds between CGA and Q[7];
ii. CGA can be sustainably released from CGA-Q[7] nanocomplex in vitro and maintain strong antioxidant activities for over 20 days;
iii. The CGA-Q[7] nanocomplex promoted osteoblast proliferation at high CGA concentrations, reduced intracellular ROS signals, and showed no increased cytotoxicity, highlighting its potential in osteoporosis treatment.

Acknowledgments

This work was supported by the Key Research and Development Program of Jiangsu Province (Social Development) Project [grant BE2022797]; Jiangsu Province Capability Improvement Project through Science, Technology and Education-Jiangsu Provincial Research Hospital Cultivation Unit (YJXYYJSDW4), Jiangsu Provincial Medical Innovation Center (CXZX202227).

Disclosure

The authors report no conflicts of interest in this work.

References

1. de Villiers TJ. Bone health and menopause: osteoporosis prevention and treatment. *Best Pract Res Clin Endocrinol Metab*. 2024;38(1):101782. doi:10.1016/j.beem.2023.101782
2. Liu J, Zhang Y, Yan W, et al. Delivery of m7G methylated Runx2 mRNA by bone-targeted lipid nanoparticle promotes osteoblastic bone formation in senile osteoporosis. *Nano Today*. 2024;54:102074
3. Guo J, Wang F, Hu Y, et al. Exosome-based bone-targeting drug delivery alleviates impaired osteoblastic bone formation and bone loss in inflammatory bowel diseases. *Cell Rep Med*. 2023;4(1):100881. doi:10.1016/j.xcrm.2022.100881
4. Mannino G, Perrone A, Campobenedetto C, et al. Phytochemical profile and antioxidative properties of Plinia trunciflora fruits: a new source of nutraceuticals. *Food Chem*. 2020;307:125515. doi:10.1016/j.foodchem.2019.125515
5. Rojas-González A, Figueroa-Hernández CY, González-Rios O, et al. Coffee chlorogenic acids incorporation for bioactivity Enhancement of foods: a Review. *Molecules*. 2022;27(11):3400. doi:10.3390/molecules27113400
6. Surma S, Sahebkar A, Banach M. Coffee or tea: anti-inflammatory properties in the context of atherosclerotic cardiovascular disease prevention. *Pharmacol Res*. 2023;187:106596. doi:10.1016/j.phrs.2022.106596
7. Han D, Gu X, Gao J, et al. Chlorogenic acid promotes the Nrf2/HO-1 anti-oxidative pathway by activating p21(Waf1/Cip1) to resist dexamethasone-induced apoptosis in osteoblastic cells. *Free Radic Biol Med*. 2019;137:1–12. doi:10.1016/j.freeradbiomed.2019.04.014
8. Naveed M, Hejazi V, Abbas M, et al. Chlorogenic acid (CGA): a pharmacological review and call for further research. *Biomed Pharmacother*. 2018;97:67–74. doi:10.1016/j.biopha.2017.10.064

9. Wang L, Zhang Y, Liu Y, et al. Effects of chlorogenic acid on antimicrobial, antivirulence, and anti-quorum sensing of carbapenem-resistant Klebsiella pneumoniae. *Front Microbiol*. 2022;13:997310. doi:10.3389/fmicb.2022.997310
10. Karadeniz F, Oh JH, Lee JI, et al. 3,5-dicaffeoyl-epi-quinic acid from Atriplex gmelinii enhances the osteoblast differentiation of bone marrow-derived human mesenchymal stromal cells via WnT/BMP signaling and suppresses adipocyte differentiation via AMPK activation. *Phytomedicine*. 2020;71:153225. doi:10.1016/j.phymed.2020.153225
11. Jia M, Nie Y, Cao DP, et al. Potential antiosteoporotic agents from plants: a comprehensive review. *Evid Based Complement Alternat Med*. 2012;2012:364604. doi:10.1155/2012/364604
12. An J, Yang H, Zhang Q, et al. Natural products for treatment of osteoporosis: the effects and mechanisms on promoting osteoblast-mediated bone formation. *Life Sci*. 2016;147:46–58. doi:10.1016/j.lfs.2016.01.024
13. Checinska K, Checinski M, Cholewa-Kowalska K, et al. Polyphenol-enriched composite bone regeneration materials: a systematic review of in vitro studies. *Int J Mol Sci*. 2022;23(13):7473. doi:10.3390/ijms23137473
14. Huang J, Xie M, He L, et al. Chlorogenic acid: a review on its mechanisms of anti-inflammation, disease treatment, and related delivery systems. *Front Pharmacol*. 2023;14:1218015. doi:10.3389/fphar.2023.1218015
15. Chen M, Sun Y, Hou Y, et al. Constructions of ROS-responsive titanium-hydroxyapatite implant for mesenchymal stem cell recruitment in peri-implant space and bone formation in osteoporosis microenvironment. *Bioact Mater*. 2022;18:56–71. doi:10.1016/j.bioactmat.2022.02.006
16. Zhang C, Li H, Li J, et al. Oxidative stress: a common pathological state in a high-risk population for osteoporosis. *Biomed Pharmacother*. 2023;163:114834. doi:10.1016/j.biopha.2023.114834
17. Yin Z, Zheng T, Ho CT, et al. Improving the stability and bioavailability of tea polyphenols by encapsulations: a review. *Food Sci Hum Wellness*. 2022;11(3):537–556. doi:10.1016/j.fshw.2021.12.011
18. Han D, Chen W, Gu X, et al. Cytoprotective effect of chlorogenic acid against hydrogen peroxide-induced oxidative stress in MC3T3-E1 cells through PI3K/Akt-mediated Nrf2/HO-1 signaling pathway. *Oncotarget*. 2017;8(9):14680–14692. doi:10.18632/oncotarget.14747
19. Wu T, Zhou Q, Hong G, et al. A chlorogenic acid-chitosan complex bifunctional coating for improving osteogenesis differentiation and bactericidal properties of zirconia implants. *Colloids Surf B Biointerfaces*. 2023;230:113484. doi:10.1016/j.colsurfb.2023.113484
20. Khatoon S, Kalam N, Shaikh MF, et al. Nanoencapsulation of polyphenols as drugs and supplements for enhancing Therapeutic Profile - A Review. *Curr Mol Pharmacol*. 2022;15(1):77–107. doi:10.2174/1874467214666210922120924
21. Li H, Xu J, Hu JF, et al. Sustained release of chlorogenic acid-loaded nanomicelles alleviates bone loss in mouse periodontitis. *Biomater Sci*. 2022;10(19):5583–5595. doi:10.1039/D2BM01099B
22. Onoue S, Yamada S, Chan HK. Nanodrugs: pharmacokinetics and safety. *Int J Nanomed*. 2014;9:1025–1037. doi:10.2147/IJN.S38378
23. Sharma S, Majumdar RK, Mehta NK. Manipulation of protein structure and bonding pattern to improve the gelling and textural quality of surimi gels from silver carp: incorporation of mosambi (Citrus limetta) peel extract. *J Sci Food Agric*. 2023;103(14):6871–6883. doi:10.1002/jsfa.12769
24. Luo Y, Liu H, Chen M, et al. Immunomodulatory nanomedicine for osteoporosis: current practices and emerging prospects. *Acta Biomater*. 2024;179:13–35. doi:10.1016/j.actbio.2024.03.011
25. Zhu H, Zheng J, Oh XY, et al. Nanoarchitecture-integrated hydrogel systems toward therapeutic applications. *ACS Nano*. 2023;17(9):7953–7978. doi:10.1021/acsnano.2c12448
26. Wu J, Shaidani S, Theodossiou SK, et al. Localized, on-demand, sustained drug delivery from biopolymer-based materials. *Expert Opin Drug Deliv*. 2022;19(10):1317–1335. doi:10.1080/17425247.2022.2110582
27. Carroy G, Lemaur V, De Winter J, et al. Energy-resolved collision-induced dissociation of non-covalent ions: charge- and guest-dependence of decomplexation reaction efficiencies. *Phys Chem Chem Phys*. 2016;18(18):12557–12568. doi:10.1039/C6CP01026A
28. Liu YH, Zhang YM, Yu HJ, et al. Cucurbituril-based biomacromolecular assemblies. *Angew Chem Int Ed Engl*. 2021;60(8):3870–3880. doi:10.1002/anie.202009797
29. Smithrud DB, Wang X, Tarapore P, et al. Crown Ether Host-Rotaxanes as Cytotoxic Agents. *ACS Med Chem Lett*. 2013;4(1):27–31. doi:10.1021/ml3003204
30. Yuan Y, Nie T, Fang Y, et al. Stimuli-responsive cyclodextrin-based supramolecular assemblies as drug carriers. *J Mater Chem B*. 2022;10(13):2077–2096. doi:10.1039/D1TB02683F
31. Gao RH, Chen LX, Chen K, et al. Development of hydroxylated cucurbit[n]urils, their derivatives and potential applications. Coord. *Chem Rev*. 2017;348:1–24.
32. Park KM, Hur MY, Ghosh SK, et al. Cucurbit[n]uril-based amphiphiles that self-assemble into functional nanomaterials for therapeutics. *Chem Commun*. 2019;55(72):10654–10664. doi:10.1039/C9CC05567C
33. Barrow SJ, Kasera S, Rowland MJ, et al. Cucurbituril-Based Molecular Recognition. *Chem Rev*. 2015;115(22):12320–12406. doi:10.1021/acs.chemrev.5b00341
34. Ghosh SK, Dhamija A, Ko YH, et al. Superacid-Mediated Functionalization of Hydroxylated Cucurbit[n]urils. *J Am Chem Soc*. 2019;141(44):17503–17506. doi:10.1021/jacs.9b09639
35. Oun R, Floriano RS, Isaacs L, et al. The ex vivo neurotoxic, myotoxic and cardiotoxic activity of cucurbituril-based macrocyclic drug delivery vehicles. *Toxicol Res*. 2014;3(6):447–455. doi:10.1039/C4TX00082J
36. Liu ZN, Hu JH, Xiong Y, et al. Supramolecular Self-assemblies of inverted cucurbit[6]uril with 1, 5-pentanediamine. *Inorganica Chim Acta*. 2023;556:121632. doi:10.1016/j.ica.2023.121632
37. Kuok KI, Li S, Wyman IW, et al. Cucurbit[7]uril: an emerging candidate for pharmaceutical excipients. *Ann N Y Acad Sci*. 2017;1398(1):108–119. doi:10.1111/nyas.13376
38. Izumiya M, Haniu M, Ueda K, et al. Evaluation of MC3T3-E1 Cell osteogenesis in different cell culture media. *Int J Mol Sci*. 2021;22(14):7752.
39. Murakami A. Dose-dependent functionality and toxicity of green tea polyphenols in experimental rodents. *Arch Biochem Biophys*. 2014;557:3–10. doi:10.1016/j.abb.2014.04.018
40. Wu M, Chen F, Liu H, et al. Bioinspired sandwich-like hybrid surface functionalized scaffold capable of regulating osteogenesis, angiogenesis, and osteoclastogenesis for robust bone regeneration. *Mater Today Bio*. 2022;17:100458. doi:10.1016/j.mtbio.2022.100458
41. Puri D. *A Prospective Utilization of Biodegradable Polymers for Controlled Drug-Delivery Applications. Bioresorbable Polymers and Their Composites*. Woodhead Publishing; 2024.

42. Jia C, Zhong Y, Zhang X, et al. Host-guest inclusion systems of nedaplatin with cucurbit[7]uril for improved in vitro antitumour activity. *J Incl Phenom*. 2020;97(1–2):99–107. doi:10.1007/s10847-020-00988-x
43. Shao P, Zhang J, Fang Z, et al. Complexing of chlorogenic acid with *β*-cyclodextrins: inclusion effects, antioxidative properties and potential application in grape juice. *Food Hydrocoll*. 2014;41:132–139. doi:10.1016/j.foodhyd.2014.04.003
44. Huang Y, Gao RH, Liu M, et al. Cucurbit[n]uril-based supramolecular frameworks assembled through outer-surface interactions. *Angew Chem Int Ed Engl*. 2021;60(28):15166–15191. doi:10.1002/anie.202002666
45. Blanco E, Shen H, Ferrari M. Principles of nanoparticle design for overcoming biological barriers to drug delivery. *Nat Biotechnol*. 2015;33(9):941–951. doi:10.1038/nbt.3330
46. Lee E-C, Kim HPark S Y.. reversible shape-morphing and fluorescence-switching in supramolecular nanomaterials consisting of amphiphilic cyanostilbene and cucurbit[7]uril. Chemistry. *Asian J*. 2019;14(9):1457-–1461
47. Zhao M, Wang H, Yang B, et al. Identification of cyclodextrin inclusion complex of chlorogenic acid and its antimicrobial activity. *Food Chem*. 2010;120(4):1138–1142. doi:10.1016/j.foodchem.2009.11.044
48. Chao J, Wang H, Zhao W, et al. Investigation of the inclusion behavior of chlorogenic acid with hydroxypropyl-β-cyclodextrin. *Int J Biol Macromol*. 2012;50(1):277–282. doi:10.1016/j.ijbiomac.2011.11.008
49. Zhang J, Coulston RJ, Jones ST, et al. One-step fabrication of supramolecular microcapsules from microfluidic droplets. *Science*. 2012;335(6069):690–694. doi:10.1126/science.1215416
50. Lee SJ, Lee JW, Lee HH, et al. Host-guest chemistry from solution to the gas phase: an essential role of direct interaction with water for high-affinity binding of cucurbit[n]urils. *J Phys Chem B*. 2013;117(29):8855–8864. doi:10.1021/jp4053874
51. Li F, Liu D, Liao X, et al. Acid-controlled release complexes of podophyllotoxin and etoposide with acyclic cucurbit[n]urils for low cytotoxicity. *Bioorg Med Chem*. 2019;27(3):525–532. doi:10.1016/j.bmc.2018.12.035
52. Xie B, Zhao H, Shui M, et al. spermine-responsive intracellular self-aggregation of gold nanocages for enhanced chemotherapy and photothermal therapy of breast cancer. *Small*. 2022;18(30):e2201971. doi:10.1002/smll.202201971
53. Guo H, Guo M, Xia Z, et al. Membrane-coated nanoparticles as a biomimetic targeted delivery system for tumour therapy. *Biomater Transl*. 2024;5(1):33–45. doi:10.12336/biomatertransl.2024.01.004